Distributed Corrosion Detection using Dedicated Optical Fiber Sensor (OFS) based Steel Rebar within Reinforced Concrete Structures by Optical Frequency-Domain Reflectometry (OFDR)

Sylvain Magne, Shamyr Ali Alvarez, Stéphane Rougeault

▶ **To cite this version:**

Sylvain Magne, Shamyr Ali Alvarez, Stéphane Rougeault. Distributed Corrosion Detection using Dedicated Optical Fiber Sensor (OFS) based Steel Rebar within Reinforced Concrete Structures by Optical Frequency-Domain Reflectometry (OFDR). European Workshop on Structural Health Monitoring (EWSHM), BINDT, Jul 2018, Manchester, United Kingdom. 23306 (12 p.). hal-04559121

HAL Id: hal-04559121
https://hal.science/hal-04559121

Submitted on 25 Apr 2024

HAL is a multi-disciplinary open access archive for the deposit and dissemination of scientific research documents, whether they are published or not. The documents may come from teaching and research institutions in France or abroad, or from public or private research centers.

L'archive ouverte pluridisciplinaire **HAL**, est destinée au dépôt et à la diffusion de documents scientifiques de niveau recherche, publiés ou non, émanant des établissements d'enseignement et de recherche français ou étrangers, des laboratoires publics ou privés.

Distributed under a Creative Commons Attribution 4.0 International License

9th European Workshop on Structural Health Monitoring
July 10-13, 2018, Manchester, United Kingdom

Distributed Corrosion Detection using Dedicated Optical Fiber Sensor (OFS) based Steel Rebar within Reinforced Concrete Structures by Optical Frequency-Domain Reflectometry (OFDR)

Sylvain Magne, Shamyr Ali Alvarez and Stéphane Rougeault
CEA, LIST, Laboratoire Capteurs Architectures Electroniques, 91191 Gif-sur-Yvette France, sylvain.magne@cea.fr

Abstract

Corrosion is a major pathology for Civil Engineering structures, affecting long-term reliability. Huge direct costs (maintenance, rehabilitation) and indirect costs (lost productivity, litigation, outages, delays, downtimes) justify strategies to minimize the impact of corrosion. Regarding civil engineering (CE) infrastructures constructed of reinforced concrete, steel reinforcing bars (rebars) are naturally corrosion-protected when embedded into concrete (pH ~ 13). Concrete carbonation ("generalized" corrosion) and chloride ion penetration ("pitting" corrosion) both accelerate their corrosion rate. Corrosion products grow in volume and the increase in pressure at the steel-concrete interface leads to cracks of the concrete layer and acceleration of degradation. They may escape as well through cracks, thus leading to a reduction in rebar diameter and global structure weakening.
Until now, inspections are carried out periodically and involve indirect measurement techniques (*e.g.* chemical-, impedance-, potential-based) that are time-consuming, costly and probabilistic in nature. Imaging techniques (*e.g.* ultrasonics) provide information about internal damage or voids within concrete but are of limited range of investigation (limited to accessible surfaces). Since it is impossible to predict where corrosion would start in large infrastructures, distributed monitoring techniques are desirable in order to early detect its onset, particularly in hidden or inaccessible areas.
We investigated the OFDR technique in the perspective of a Condition-Based Maintenance (CBM), identified as a future challenge in order to provide safe operating conditions and cost savings. The use of telecom-grade fibers as sensors is motivated by their cost-effectiveness, electrochemical passivity, electromagnetic immunity and networking/multiplexing capability.
We report on an original fiber-based corrosion sensor design employing usual steel rebars in order to avoid galvanic corrosion to occur. Since the sensor is a rebar, it also behaves as an extensometer and a dedicated design is proposed to discriminate between global thermomechanical loadings and local corrosion mechanical effects. Changes in OFDR signals with respect to reference signals provide localization, identification and direct measurement of corrosion. The sensing device was successfully tested under accelerated pitting corrosion as a proof-of-concept.

1. Introduction

According to the World Corrosion Organization (WCO), the direct cost of corrosion amounts to approximately $USD 1.8 trillion, *i.e.* 3-4 % of GDP (Gross Domestic Product) of all industrialized countries (1). The last study about corrosion cost was published in 2001 by the US Federal Highway Administration (FHWA) with support from NACE International (National Association of Corrosion Engineers) (2). This study estimated that the annual direct cost due to corrosion (from all industry sectors) amounts

Creative Commons CC-BY-NC licence https://creativecommons.org/licenses/by-nc/4.0/

to $USD 276 billion. Indirect costs (lost productivity, litigation, outages, delays, downtimes) were estimated to be equal to direct cost, so that the global cost of corrosion was actually estimated to be twice the value reported in (2). The direct corrosion cost for infrastructures (highway bridges, transmission pipelines, waterways & ports, HAZMAT storage, airports, railroads) was estimated to be $USD 22.6 billion.

The cost of corrosion of Civil Engineering (CE) infrastructures constructed of reinforced concrete was not given in details in the study. However, 83 % of the US bridges are made of concrete and 15 % were considered as structurally deficient at the time of the study (1999-2001) (1). Besides, indirect costs were estimated to be ten times higher than direct costs for highway bridges.

In France, the annual cost for monitoring, maintenance and rehabilitation exceeded 0.5 billion Euros in 1999 (3).

Concrete is a low-cost material heavily used for construction but of poor mechanical resistance compared to other construction materials (*e.g.* metals, carbon/glass fiber-reinforced plastics). Steel reinforcing bars (rebars) are used to improve the tensile strength of concrete. The highly alkaline pH of concrete (~ 13) leads to the passivation of the steel interface that protects the material against corrosion (4).

Atmospheric carbon dioxide contributes to decrease the pH value (corrosion starts at pH ~ 11.5) leading to concrete carbonation ("generalized" corrosion). The other dominant corrosion mechanism is "pitting" corrosion of rebars by chlorides, that concerns structures located in marine environments or exposed to deicing salts.

Both mechanisms dramatically accelerate the corrosion rate. Corrosion products eventually grow in volume and the increase in pressure at the steel-concrete interface leads to cracks of the concrete layer and acceleration of degradation. Corrosion products may escape as well through cracks, thus leading to a reduction in rebar diameter and global structure weakening.

Solutions for preventing corrosion failures, such as using corrosion-resistant alloys, or mitigating the corrosion impact (protective paints, application of cathodic protection), are costly and usually restricted to prestige monuments (*e.g.* Eiffel Tower in Paris, France). According to the code for design for durability (5), monitoring becomes a part of the design and construction process. Scheduled-driven inspections are carried out during the life of the structure in order to detect major degradations impairing its integrity and endangering safety. Most NDT (Non-Destructing Testing) techniques used for concrete CE works detect a corrosion risk rather than the corrosion impact itself or by-products of the corrosion reaction. These monitoring techniques consist in measuring the environmental species or conditions that are precursors of the corrosion process. They involve chemical analysis (*e.g.* pH, chloride concentration, etc.) (6), or resistivity, impedance- or half-cell potential-based detection (7).

Direct monitoring techniques are able to detect either by-products of the corrosion reaction of its mechanical impact over the structure. Among these methods, imaging techniques such as ultrasonic pulse velocity (8) and more recently backscattered computed radiation tomography (9), are used. These techniques require scanning huge amounts of surface (hundreds of m^2 and more) by an operator equipped with either a hand-held or motorized monitoring device. The process is tedious, time-consuming and costly. Moreover, structure downtime (*e.g.* traffic interruption) is often imposed for safety reasons during periods of inspection. Finally, these techniques are often of limited range of investigation (restricted to accessible surfaces) and hidden or inaccessible parts fall out of sight so that the global damage is often underestimated.

2. Optical Fiber Sensor for *in situ* corrosion detection within concrete

Several Optical Fiber Sensors (OFS) were investigated as means for *in situ* direct corrosion detection within concrete structures.

2.1 Color sensor

P.L. Fuhr and D. R. Huston (10) investigated a fiber sensor based on color change. The authors recorded spectra of the light reflected back by the rebar surface for both states (metallic and rusted) and provided data analysis to retrieve the corrosion state. The sensor is simple and low cost but distributed measurements seem difficult to achieve (the detection is localized at the extremity of the fiber).

2.2 Sacrificial thin film

Other others investigated sacrificial thin films assumed as representative of a rebar. For instance, C.K.Y. Leung *et al.* (11) investigated a fiber reflector with a sputtered iron film deposited on fiber end face. Several limitations are associated with this concept: (i) the sensor is not amenable to multiplexing on a single fiber, (ii) the absence of intensity reference leads to the impossibility to discriminate between corrosion effect and transmission loss (*e.g.* due to connector aging), and (iii) the electrochemical potential of the sputtered film is not equivalent to that of the rebar steel.
Martins-Filho *et al.* (12) proposed a quasi-distributed version of this concept with multiple fiber-ends, connected to a lead fiber with optical couplers, and interrogated with an OTDR (optical time-domain reflectometer) device. The OTDR device also provides a reference baseline from Rayleigh scattering, enabling self-intensity referencing.
A galvanic corrosion between the sensor and rebars may occur within the structure on account of the different electrochemical potentials of rebars and sensor. Therefore, if the sensor corrodes faster than the rebars, it leads to a false alarm. Inversely, if the sensor does not experience corrosion or much later than the rebar does, the sensor is inoperant.

2.3 Fiber Bragg Gratings (FBGs)

Fiber Bragg Gratings (FBGs) were investigated as well for corrosion detection by several authors. For instance, N. Zhang *et al.* (13) proposed a FBG photowritten within a taper coated with a sputtered iron film. Variations in spectral shape are related to corrosion-induced refractive index changes.
J-R. Lee *et al*. (14), S.K.T. Grattan *et al*. (15), Z. Zheng *et al.* (16) and S. Ali Alvarez *et al.* (17) evaluated FBG corrosion sensors relying on corrosion-induced strain variations, either a strain release induced by pitting corrosion or strain increase due to expansion of corrosion products.
J-R. Lee *et al.* (14) used a FBG prestrained on a sacrificial metal sample. The observed Bragg shift was due to the corrosion-driven reduction in rigidity (loss of mass and section) of the sample. The sensor prototype was a laboratory specimen, not properly packaged for embedment within concrete.

Z. Zheng *et al.* (16) and S.K.T. Grattan *et al.* (15) both developed a FBG corrosion sensor directly bonded onto the rebar material. Bragg shifts were observed because of strain induced by expansion of corrosion products.

Z. Zheng *et al.* (16) mechanically polished the surface of a 20-mm long part of a rebar and bonded an FBG along an orthoradial orientation (*i.e.* within a section of the rebar). The FBG was then protected by a Fiber-Reinforced plastics (FRP) foil. The corrosion sensor prototype was embedded in a concrete cube (edge = 150 mm) and submitted to a generalized corrosion after a 7-day cure (immersion into soda and salter water, current = 0.2 A). Since corrosion products could not escape, they accumulated at the concrete-rebar interface and increased in volume. The resulting increase in pressure and strain eventually led to concrete break. No indication of corrosion was observed during the first 15 days. During the last three days, the Bragg shift increased rapidly up to 3 nm before concrete broke (relative increase of rebar diameter of 0.25 %).

This experiment provides a proof-of-concept for the Bragg detection of generalized corrosion of a rebar but the winding procedure may prove difficult on small-diameter rebar (*e.g.* 5 to 6 mm) due to bending-induced loss and mechanical fatigue. Moreover, the large FRP protection prevents the corrosive species to attack the surface nearby the FBG thus causing a time delay between the onset of corrosion and its detection.

S.K.T. Grattan *et al.* (15) performed two types of corrosion testing on a steel rebar (length = 750 mm, diameter = 12 mm) with bonded FBGs (along rebar axis) and electrical resistance strain gauges (ERSGs). The first test was performed in a salt spray chamber projecting a solution of salted water (0.05 %wt, T = 35°C, RH = 85 %). FBGs experienced small strains (~ 500 microstrain) after delay times varying from 37 days up to 76 days. The second test consisted in embedding the sensor into a concrete block and to accelerate corrosion by the appliance of a current. The rebars protuded from the block and rust seeping was observed along the rebar. A first FBG experienced positive strains (1700 microstrain) while another experienced negative strains (-1200 microstrain). This test was partly conclusive probably on account of the fact that corrosion products could escape the concrete block along the rebar.

S. Ali-Alvarez *et al.* (17) performed similar experiments to those of Zheng *et al.* (16) and Grattan *et al.* (15) in both pitting and generalized corrosion schemes. The rebar material was a E-500 type steel and the fiber was bonded inside a groove with an epoxy of high curing temperature (Tc ~ 80°C). Once the bonding was effective on the rebar surface, the fiber was strained during cooling down at room temperature since the coefficient of thermal expansion (CTE) of iron ($1.2\ 10^{-5}\ K^{-1}$) is higher than that of silica ($5.10^{-7}\ K^{-1}$). The Bragg shift is given by the relation:

$$\frac{\Delta\lambda}{\lambda} = (\xi + (1 - p_e) \cdot CTE) \cdot \Delta T \qquad (1)$$

where ξ is the thermo-optic coefficient of silica and $p_e \sim 0.21$ is the photo-elastic constant of the FBG (under axial strain).

For all corrosion experiments, electrochemical potentials were measured with a VoltaLabPGZ-100 device and a Burleigh/EXFO WA-7600 wavemeter was used for recording the Bragg spectra (spectral resolution ~ 15 pm). For a temperature shift of 70°C, a Bragg shift of -1.44 nm (@1530 nm) was experimentally observed between step #1 (before bonding : @1530.086 nm, 25 °C) and step #3 (after bonding : 1528.650 nm, 25°C) which corresponds to a compressive strain of about -1200 µstrain.

A pitting corrosion was performed in salted water (35 g/l) under an applied current density of 70 $mA.cm^{-2}$. Rust breaks off and loses its mechanical integrity. As the corrosion advances, the remaining part of uncorroded metal surface diminishes progressively with time and so does the epoxy-metal bonding joint that is under stress (pullback force by the silica fiber). The bonding joint experiences an increase in strain due to the reduction in bonded surface and eventually releases the stress (bond break). The Bragg wavelength therefore increased until it finally went back to its initial value (unbonded). Is it important to notice that the strain release did not follow an "all or nothing" behavior but rather evolved continuously with time, yielding potential indication about the progression of the corrosion reaction.
Another corrosion sensor of same kind was then embedded into a mortar solid cube (Portland, 6 x 6 x 7 cm^3) and submitted to an accelerated generalized corrosion. After a 7-day cure, the concrete sample was then immersed in a salted water solution with soda and a current density of 100 $mA.cm^{-2}$ was applied to the mortar. In this second configuration the internal pressure at rebar-concrete interface was expected to increase on account of the expansion of corrosion products at the rebar surface. During the first 3 days of experiment, the Bragg wavelength remained stable and began to drop since the fourth day. The mortar sample got fractured on the sixth day. The maximum recorded Bragg shift was about -220 pm ± 50 pm which translates into an internal pressure of about 50 MPa ± 11 MPa (-4.4 pm/MPa @1530 nm). This value is higher than the standard tensile strength of concrete (~ 3 to 5 MPa). A physical explanation might be a partial strain transfer along the grating length that would account for a Bragg shift larger than expected.
The detection of the corrosion-induced strain as demonstrated in (14-17) stems as a pertinent approach for direct corrosion detection in a future Condition-Based Maintenance (CBM) strategy. However, the number of FBGs that would be needed to cover a CE structure is huge (several thousands). Both sensor and deployment costs are thus likely to exceed the maintenance budget allocated for by the owner of the CE structure which hinders the spread of this technique.

2.4 BOTDA (Brillouin Optical Time Domain Analysis)

Since it is impossible to predict where corrosion would start in large infrastructures, distributed monitoring techniques are desirable in order to early detect its onset, particularly in hidden areas, while keeping cost at a reasonable value.
With this aim in view, the BOTDA technique has been investigated as a distributed corrosion monitoring, relying on the strain induced by expansion of corrosion products (18-19). The accuracy in strain measurement is approximately 20 microstrains (to be compared to that of FBG measurements that is currently about 1 microstrain or less). The spatial resolution of BOTDA measurements is about 1 meter. Therefore, the fiber was wound around the steel rebar in order to provide a local corrosion measurement (several centimeters) which complicates the deployment and increases the sensor cost. This concept cannot be applied on small-diameter rebars (less than 10 mm) on account of large bending-induced light loss and mechanical fatigue. The authors observed a continuous rise of the longitudinal strain due to expansion of corrosion products up to 1000 microstrains (19). The BOTDA recordings were limited by the low signal-to-noise ratio (SNR) of the Brillouin signals at the end of the experiment.

3. Fiber-based steel rebar corrosion sensor prototype

The OFDR (Optical Frequency-Domain Reflectometry) technique is another interesting solution in a perspective of CBM because it provides a distributed monitoring capability with metrological performance equivalent to FBGs.
The use of telecommunication-grade fibers as sensors is motivated by their cost-effectiveness, electrochemical passivity, electromagnetic immunity and networking/multiplexing capability. Furthermore, a single interrogation unit may be moved from one site to another in order to improve the pay-back for the OFDR unit.
We investigated a direct distributed corrosion sensor prototype interrogated by OFDR in the perspective of CBM, with the aim to determine inspection intervals more accurately and to prioritize corrosion-prevention strategies in a context of spending restrictions.
The principle of OFDR is well documented (20) and will not be recalled in this paper. Backscattered profiles are obtained by inverse Fourier Transform of the interference pattern recorded during laser tuning and the spatial resolution is about 10 micrometers for a tuning range of 80 nm. The distributed strain/temperature profiles are obtained by cross-correlation of backscattered profiles with a reference one, recorded at known strain and temperature. The cross-correlation is performed over fiber segments ("gauge length") typically one-centimeter long or less, equivalent to the spatial resolution for metrological applications. The relative frequency shift between cross-correlated profiles is identical to the relative Bragg shift of FBGs, according to:

$$\frac{\Delta\nu}{\nu} = -\frac{\Delta\lambda}{\lambda} \tag{2}$$

Based upon Eq (2), the frequency shift $\Delta\nu$ (in GHz) depends on the longitudinal strain ε (in microstrain) by the relation:

$$\Delta\nu = -0.151\ (GHz/microstrain) \cdot \varepsilon \tag{3}$$

3.1 Conception of the corrosion sensor

The corrosion sensor prototype is built from a steel rebar (Fe-500, ∅ = 13 mm, L = 300 mm) to avoid galvanic corrosion to occur and not to weaken the structure. Since the corrosion sensor also participates to the reinforcement, it behaves as an extensometer and provides additional information about internal structure loading and presence of cracks (stress discontinuity along rebar length). On the other hand, local corrosion mechanical effects superimpose over global thermomechanical loading. A discrimination of both effects is therefore necessary and achieved with the help of an original design based on the periodic succession of corrosion-protected and unprotected surfaces (period = 50 mm), as depicted in fig. 1. Corrosion-protected parts (epoxy layer) serve as strain reference and account only for thermomechanical loading. The other parts (unprotected) are prone to corrosion damage and provide short-scale (local) strain effects that are discriminated against the global (large scale) loading.
The corrosion sensor prototype manufactured by the CEA-LIST is shown on fig. 2.
The optical fiber (SMF28) was inserted within a groove machined on rebar surface, along its axis. The fiber was bonded with a high-cure temperature epoxy according to same protocol as described in references (17, 21-22). When cooled down at room

temperature, the fiber is strained in compression (about -1200 µstrain for ΔT = 70°C). The equivalent frequency shift is 181 GHz (according to Eq (3)). It is important to bear in mind that a positive frequency shift means a negative strain (compression). Conversely, a negative frequency shift means a positive strain (traction).

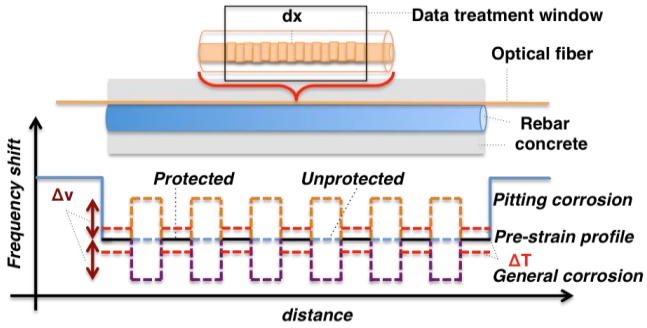

Figure 1. Design concept of the fiber-based rebar corrosion sensor prototype

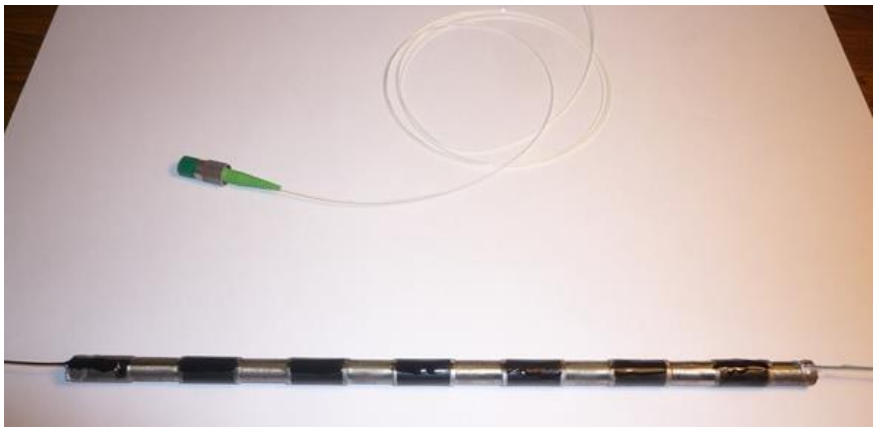

Figure 2. View of the corrosion sensor prototype with successive protected and unprotected segments for discrimination of short-scale corrosion-induced mechanical effects from global thermomechanical loading

4. Experimental

4.1 Accelerated corrosion conditions

An accelerated pitting corrosion experiment was performed with a current generator (constant applied current = 180 mA). The sensor prototype was immersed into a water tank (aquarium) filled with salted water (1.4 g/l). A copper clamp connected the corrosion sensor to the anode while a copper electrode was connected to the cathode.
The theoretical corrosion rate is given by the Faraday law:

$$CR_m^{th} = \frac{dm}{dt} = -I \cdot M/(n \cdot F) \qquad (4)$$

where M = 55.84 g/mol is the atomic mass of the metal (iron), I is the current (in A), n is the number of electrons exchanged in the corrosion reaction (n = 2) and F =e.N_A = 96400 C/mol is the Faraday charge constant (e is the electron charge and N_A is the Avogadro number).

4.1.1 Test condition on dummy sensor

A dummy sensor was submitted to accelerated corrosion in order to validate the Faraday law in the context of the experiment. The initial mass of the dummy rebar was 120.998 g (± 1 mg). The calculation (Eq (4)) gives a mass corrosion rate of -0.187 g/h (the amount of lost mass was 15.13 g at the end of the experiment). It follows that the relative mass corrosion rate was $CR_m^{th} = -0.1545 \cdot \%/h$.

The experimental corrosion rate was estimated by weight loss measurement.

The operating mode consisted in applying the nominal current (180 mA) over the dummy sensor (of same dimensions as the rebar prototype) immersed in salted water for several hours. Then, the current was stopped and the rebar was removed from the water. Corrosion products were then scrapped off the surface and the rebar was weighted. The rebar was then replaced into the water to pursue the corrosion process.

Fig. 3 shows the plot of the relative loss of rebar mass with respect to time. It exhibits a linear trend indicating that the corrosion rate was not significantly slowed by diffusion through the thickness of corrosion products over a time scale of several hours.

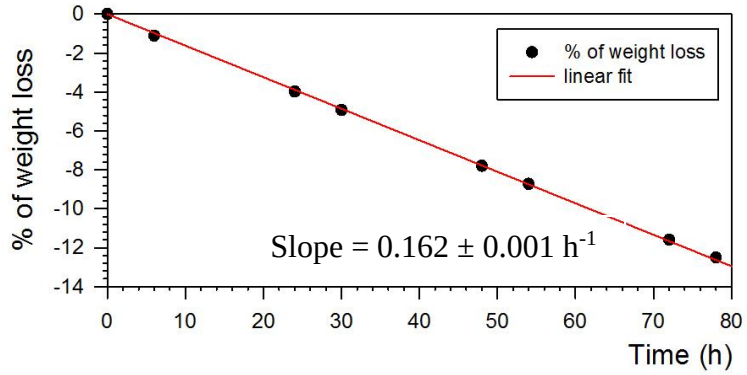

Figure 3. Percentage of corrosion-induced weight loss *vs* time and estimation of the relative mass corrosion rate in accelerated conditions

The experimental mass corrosion rate was $CR_m^{exp} = -0.162 \cdot \%/h$ which is very close to the theoretical value and validates the calculation.

Taking into account circular symmetry of the rebar geometry, the mass corrosion rate CR_m may be related to the corrosion rate by the simple relation:

$$CR_m = \frac{1}{m}\frac{dm}{dt} = \frac{2}{r}\frac{dr}{dt} = 2 \cdot CR \qquad (5)$$

where m is the mass and r is the radius of the rebar.

The relative corrosion rate CR is then about $8.10^{-4}\ h^{-1}$ (0.08 %.h^{-1}) which corresponds to 3,6 µm/h for a radius of 4.5 mm. Since the corrosion rate in marine environments is about 0.1 mm/year (0.011 µm/h) (1), the acceleration factor is about 330.

4.1.2 Test condition for the corrosion sensor

The experiment is shown in fig. 4. Only the exposed surface of the corrosion sensor was prone to corrosion and taken into account in the exposed surface that is about 49.5 cm^2. A current of 180 mA was applied to the corrosion sensor and the current density was about 3.6 mA.cm^{-2}. The volume of the corrosion sensor is about 9.8 cm^3 which corresponds to a mass of metal of 77 g (7.87 g/cm^3). The mass corrosion rate is the same as in 4.1.1 since the applied current was the same, *i.e.* 0.187 g/h. The relative mass

corrosion rate is then about 0.24 %.h^{-1}. The relative corrosion rate is then 0.12 %.h^{-1} which corresponds to 5.4 µm/h for a radius of 4.5 mm.

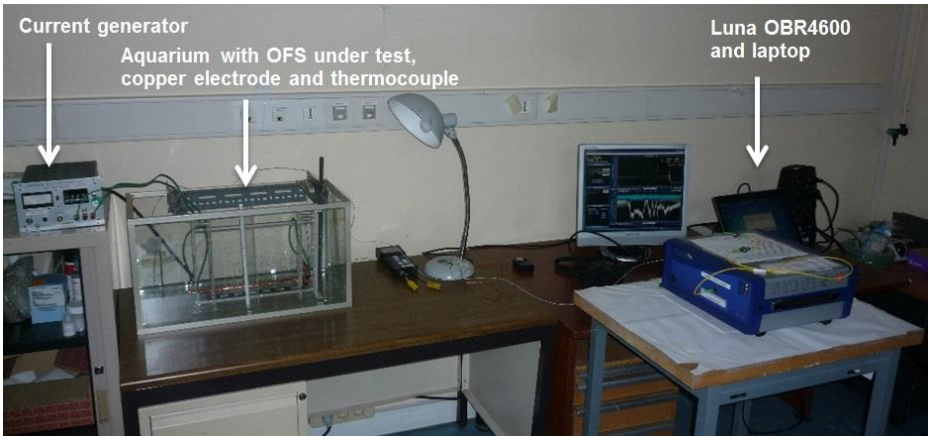

Figure 4. View of the experimental set-up for pitting corrosion

During the corrosion test, the copper electrode was not put parallel to the rebar sensor and the electric field between the copper electrode and the rebar was not constant with respect to fiber position. The practical consequence is that the corrosion rate was not constant either and we initiate a traveling corrosion from the extremity of the rebar towards the interior part (positions: 4.02 m, 4 m, 3.94 m). The other consequence is the apparition of several time delays between the beginning of the experiment and onsets of corrosion for successive parts of the rebar. During the experiment, a thermocouple was immersed nearby the corrosion sensor in order to monitor temperature changes (the temperature was kept constant within ±1°C during the whole experiment).

4.2 Distributed corrosion monitoring along the rebar-based sensor

4.2.1 OFDR protocol

The following Luna's parameters (OBR4600) were used for the experiment: Sensing range = 0.8 cm, gage length = 0.5 cm, sensor spacing = 0.1 cm.
A reference backscattering trace was first recorded at the beginning of the experiment, before switching on the current generator. Then, the current was applied continuously and several OFDR traces were recorded along at given periods of time. The current generator has been switched off outside working hours (evening and night).
Cross-correlations were performed by the Luna software in order to retrieve the changes in strain profiles along the rebar-based sensor as corrosion advanced.

4.2.2 Evolution of strain profiles with pitting corrosion

Fig. 5 shows the strain profiles along the rebar-based sensor obtained by cross-correlation of backscattered traces with the reference one, taken before appliance of the current. This figure shows the time evolution of the frequency shift (proportional to strain release) as an indicator of the progression of corrosion.
As rust surface increases, the proportion of metallic surface diminishes accordingly and the fiber strain is progressively released, similarly to previous experiments (15, 18).
After the first segment being corroded, a new reference trace has been recorded. A second set of strain profiles was produced and the evolution of the corrosion of the second segment nearby is shown in fig. 5b.

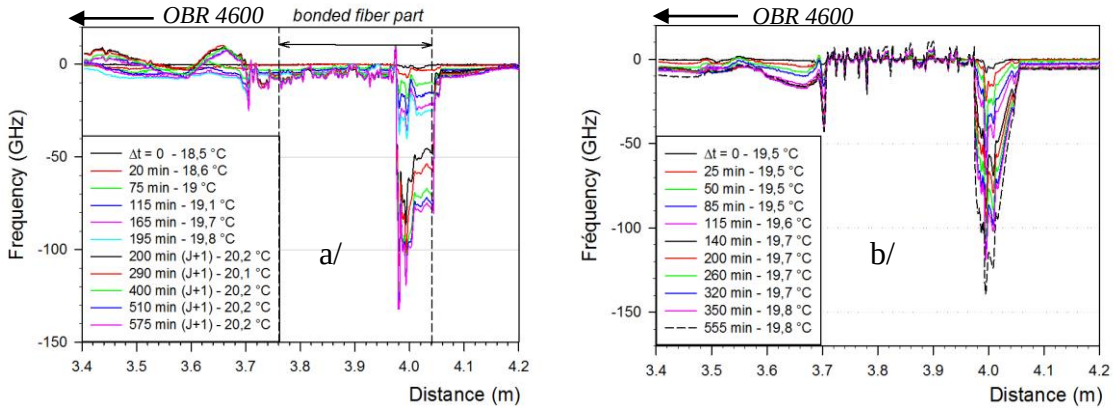

Figure 5. Evolution of the strain profile along the sensor length monitored by the OFDR technique, evolution along the a/ first segment being corroded, b/ second segment being corroded

In this case, the first corroded segment is no longer apparent since the fiber strain was released to zero.

As previously considered (16-18), the frequency shift is progressive which opens the way to the monitoring of the time evolution of the corrosion process. Indeed, the Fig. 6 shows the amplitude of the fiber strain over the successive segments attacked by corrosion. The strain evolution with respect to time exhibits a $t^{1/2}$ dependence that may indicate a diffusion-limited reaction due to the presence of corrosion-products at the interface slowing down the corrosion reaction.

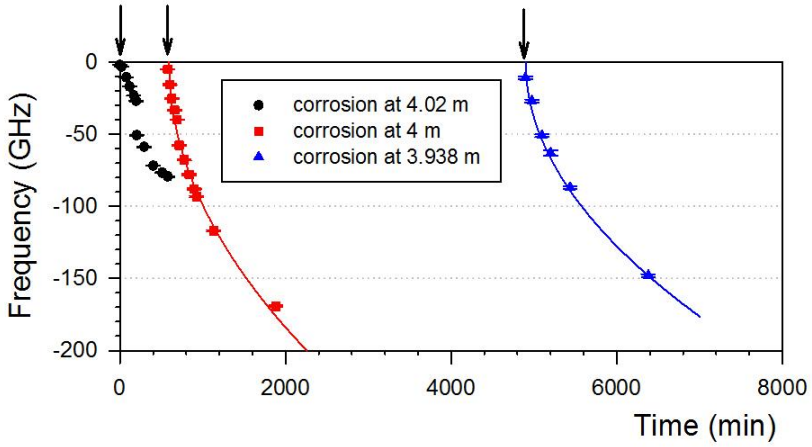

Figure 6. Evolution of the amplitude of strain monitored *vs* time for each of the three corroded segments, showing a $t^{1/2}$ dependence typical of a diffusion-limited kinetics.

The experiment has been discontinued for the 1st segment and the two series of data for the segment at 4.02 m are not in continuity. The 2nd and 3rd sets of frequency data were recorded without time interruption and the strain evolution *vs* time is modeled by the relations (6) and (7) for the 2nd (4 m) and 3rd (3.938 m) segments respectively.

$$F_2(GHz) = -4.9.\sqrt{t(min) - 590\ min} \quad (6)$$

$$F_3(GHz) = -3.85.\sqrt{t(min) - 4900\ min} \quad (7)$$

The experiment was stopped after 108 hours of pitting corrosion.

5. Conclusions

A corrosion sensor prototype has been manufactured according to an original segmented design, alternating covered (corrosion-protected) and uncovered sections (corrosion-sensitive) with the aim to discriminate global thermomechanical loadings from short-scale corrosion effects. As a rebar, the corrosion sensor participates to structure reinforcement and prevents any galvanic corrosion with other rebars (same electrochemical potential).

In this work, we investigated the OFDR technique as a distributed strain monitoring technique involving low-cost telecommunication-grade optical fibers as sensors. The fiber is epoxy-bonded at high temperature onto the steel rebar and strained in compression at room temperature. Submitted to pitting corrosion, the strain was progressively released following the extension of rust with time. The time evolution of strain followed a $t^{1/2}$ dependence that is typical of a diffusion-limited corrosion kinetics.

Changes in OFDR strain data provide centimetric localization, identification and direct measurement of corrosion. This distributed monitoring technique is thus suitable to structural Health Monitoring (SHM) in hidden or inaccessible zones inside reinforced concrete structures since it is not possible to predict where corrosion would start in large infrastructures. Furthermore, the direct corrosion detection capability lends itself to Condition-Based Maintenance (CBM), by contrast to other indirect methods that convey probabilistic estimation of a corrosion risk. The sensing device was successfully tested under accelerated pitting corrosion as proof-of-concept. In a previous work (21), we have experimented this concept in generalized corrosion as well.

Finally, the mechanical protection of the fiber was restricted to a thin epoxy ribbon (1 mm width) with the aim to minimize the delay for reaction of the corrosion sensor, as evidenced by several authors (15-17). Therefore, the epoxy ribbon does not prevent corrosion from progressing nearby the fiber, minimizing the delay time between the trigger of the corrosion reaction and the observation of the OFDR change.

The future perspective is to provide tests in concrete structures with global and local loadings in order to check the performance in real CE conditions.

Acknowledgements

The authors would like to thank Dr Valérie L'Hostis (CEA/DEN/DPC/SCCME/LECBA) for sharing its expertise in corrosion science and electrochemical measurements and Dr P. Ferdinand for co-supervision of the work of S. Ali-Alvarez.

References

1. G. Schmitt, M. Schütze, G.F. Hays, W. Burns, E-H. Han, A. Pourbaix, G. Jacobson, "Global needs for knowledge dissemination, R&D in materials deterioration and corrosion control", World Corrosion Organization, White paper, 2009.
2. G. H. Koch, M.P.H. Brongers, N.G. Thompson, P. Virmani, J.H. Payer, "Corrosion cost and prevention strategies in the US", U.S. Department of Transportation, Federal Highway Administration, Report FHWARD-01-156, 2002.
3. E.H. Rochdi, "Contribution à l'analyse du comportement mécanique de dalles en béton armé renforcées par matériaux composites", PhD. Thesis, N° 282-2004.

4. V. L'Hostis, F. Foct, P. Dillmann, “Corrosion behaviour of reinforced concrete: Laboratory experiments and archeological analogues for long-term predictions", J. Nucl. Mat. **379**, pp. 124-132, 2008.
5. EUROCODE 2, "Design of concrete structures – part 1: General rules and rules for buildings, European Committee for standardization", CEN, EN1992-1-1, 2004.
6. M. Sun, W.J. Staszewski and R.N. Swamy, “Smart sensing technologies for SHM of Civil Engineering structures”, Int. J. adv. Civ. Eng., ID 724962, 2010.
7. L. Bertolini, B. Elsener, P. Pedeferri, E. Redaelli and R. Polder, “Corrosion of steel in concrete – prevention, diagnosis and repair”, Wiley, 2nd Ed., 2014.
8. T.S.T Amran, M.P. Ismail, M.A Ismail, M.S.M. Amin, M.R. Ahmad and N.S.M. Basri, “GPR application on construction foundation study”, IOP Conf. Ser.: Mater Sci. Eng. **271**, 012089, 2017.
9. D. Constantinis, “Radiation backscatter-based non-destructive technology detects corrosion under insulation on offshore oil and gas platforms”, Mater. Performance **53** (5), pp. 14-16, 2004.
10. P. Fuhr and D.R. Huston, “Corrosion detection in reinforced concrete roadways and bridges *via* embedded FOS”, Smart. Mater. Struct. **7**, pp. 217-228, 1998.
11. C. K. Y. Leung, K. T. Wan and L. Chen, “A novel optical fiber sensor for steel corrosion in concrete structures”, Sensors **8** (3), pp. 1960–1976, 2008.
12. J. F. Martins-Filho, E. Fontana, J. Guimarães and I. J. Souza Coêlho, “Multipoint fiber-optic-based corrosion sensor”, 19th Optical Fiber Sensor conference (OFS), Perth (Australia), SPIE **7004**, pp. 70043P, 2008.
13. N. Zhang, W. Chen, X. Zheng, W. Hu, M. Gao, “Optical sensor for steel corrosion monitoring based on etched FBG sputtered with iron film”, IEEE Sensors J. **15** (6), pp. 3551-3556, 2015.
14. J.-R. Lee, C.-Y. Yun, et D.-J. Yoon, “A structural corrosion-monitoring sensor based on a pair of prestrained FBG”, Meas. Sci. Technol. **21** (1), 017002, 2010.
15. S. K. T. Grattan, S. E. Taylor, T. Sun, P. A. M. Basheer and K. T. V. Grattan, “Monitoring of Corrosion in Structural Reinforcing Bars: Performance Comparison Using In Situ Fiber-Optic and Electric Wire Strain Gauge Systems”, IEEE Sensors J. **9** (11), pp. 1494-1502, 2009.
16. Z. Zheng, X. Sun and Y. Lei, “Monitoring corrosion of reinforcement in concrete structures via FBG sensors”, Front. Mech. Eng. China **4** (3), p. 316-319, 2009.
17. S. Ali-Alvarez, P. Ferdinand, S. Magne and R.P. Nogueira, “Corrosion detection and evolution monitoring in reinforced concrete structures by the use of FBG Sensor”, SPIE **8692**, pp. 86924U1-7, 2013.
18. X. Zhao, P. Gong, G. Qiao, J. Liu, X. Lv and J. Ou, “Brillouin corrosion expansion sensors for steel reinforced concrete structures using a fiber optic coil winding method”, Sensors **11**, pp. 10798-10819, 2011.
19. H. Wei, X. Zhao, X. Kong, P. Zhang, Y. Cui and C. Sun, “The performance analysis of distributed Brillouin corrosion sensors for steel reinforced concrete structures”, Sensors **14**, pp. 431-442, 2014.
20. B. Soller, D. Gifford, M. Wolfe and M. Froggatt, “High resolution optical frequency domain reflectometry for characterization of components and assemblies”, Opt. Express **13** (2), pp. 666–674, 2005.
21. S. Ali-Alvarez, P. Ferdinand, S. Magne and R.P. Nogueira, “OFS for Corrosion Detection and Evolution Monitoring in Reinforced Concrete Structures”, Int. Conf. on Structural Health Monitoring (IWSHM), Stanford, 2013.